Numerical Experiments of Axisymmetric Flow in a Nonuniform Gravitational Field

Michele G. Macaraeg*
NASA Langley Research Center, Hampton, Virginia

A numerical study of the steady, axisymmetric flow in a heated, rotating spherical shell is conducted to model the Atmospheric General Circulation Experiment (AGCE) proposed to run aboard a later Shuttle mission. The AGCE will consist of concentric rotating spheres confining a dielectric fluid. By imposing a dielectric field across the fluid, a radial body force will be created. The numerical solution technique is based on the incompressible Navier-Stokes equations. In the method, a pseudospectral technique is used in the latitudinal direction; a second-order-accurate finite-difference scheme discretizes time and radial derivatives. The performance of this numerical scheme is discussed for the AGCE, which has been modeled in the past only by pure finite-difference formulations. In addition, previous models have not investigated the effect of using a dielectric force to simulate terrestrial gravity. The effect of this dielectric force on the flowfield is investigated, as well as the effects of varying rotation rates and boundary temperatures. Among the characteristics noted are the production of larger velocities and enhanced reversals of radial temperature gradients for a body force generated by the electric field. Correlation among flowfields with uniform, inverse-square and inverse-quintic force fields is obtained using a modified Grashof number.

Introduction

SINCE the nineteenth century there have been experimental efforts aimed at better understanding the Earth's atmosphere. Until the 1950s, however, these efforts were qualitative in nature. It was found that experiments involving a fluid confined between two concentric, rotating cylinders could be systematically studied. Experiments performed by Hide[1] in 1953, using a cylindrical annulus, resulted in the discovery of a meandering jet that greatly resembled the earth's jet stream. In 1965, Fowlis and Hide[2] quantitatively produced a flow regime diagram by careful measurements taken from the annulus experiments. Figure 1 is the regime diagram adapted from Fowlis and Hide. The ordinate is a thermal Rossby number, and the abscissa a Taylor number, which are given as

$$\mathrm{Ro}_T = ag\Delta T d/\Omega^2(r_0 - r_i)^2 \tag{1}$$

$$\mathrm{Ta} = 4\Omega^2(r_0 - r_i)^5/\nu^2 d \tag{2}$$

where g is the acceleration due to gravity, a the thermal expansivity, ΔT the horizontal temperature difference, d the annulus height, $(r_0 - r_i)$ the radial thickness, Ω the rotation rate, and ν the kinematic viscosity. The knee-shaped curve in Fig. 1, referred to as the critical curve, separates the axisymmetric flow regime from the wave-like flow (nonaxisymmetric regime).

The flow in the nonaxisymmetric regime is an analog of the synoptic scale motion of a planetary atmosphere. The annulus experiments have therefore guided studies concerning the predictability or periodicity of the atmosphere. Scaling of the governing equations based on large-scale features of the atmosphere and laboratory experiments leads to the same set of approximate equations for both systems. Thus, the experiments are models of the synoptic-scale atmospheric flow.

Since analytical solutions are not obtainable due to the strong nonlinearity of the governing equations, numerical modeling has served to enhance the theory and provide a quantitative comparison with experiment. Although models are becoming increasingly more complex, substantial advances in atmospheric studies have come from simple models which have isolated essential mechanisms concerning the Earth's general circulation. It was observed by Lorenz[3] that a steady axisymmetric solution to the governing equations exists everywhere in parameter space. The reason for the nonaxisymmetric regimes is the instability of the axisymmetric flow to infinitessimal (nonaxisymmetric) perturbations. The first step, therefore, in determining whether a given flow is stable is to calculate the steady, axisymmetric states. If a given axisymmetric solution is unstable to perturbations of any wavelength, then it might not be observed in a physical situation. Axisymmetric states for the thermally driven motion of a fluid contained in a rotating cylindrical annulus were numerically investigated by Williams.[4,5] Axisymmetric states were thoroughly studied, but a variety of points in parameter space were not considered. Miller and Gall[6] used a linear model to predict a transition curve very close to that observed in the laboratory.

An obvious disadvantage of cylindrical models of the Earth's atmosphere is the geometrical difference. However, experimental studies done in a spherical geometry on Earth cannot generate a radial body force strong enough to compete with terrestrial gravity. Such an experiment needs the near zero gravity of Spacelab to generate a sufficiently dominant radial body force.

The numerical model in this study will serve as an aid in constructing a regime diagram for a spherical geometry, analogous to the cylindrical annulus case (Fig. 1). The spherical regime diagram is also most essential for the Atmospheric General Circulation Experiment (AGCE), since knowing the location of the axisymmetric and nonaxisymmetric flow regimes is necessary for the design of the AGCE instrument.

In addition to the need for a spherical regime diagram, it is desirable for AGCE to know the effect of the radial variation of the dielectric gravitational field. The radial force

Received April 23, 1985; presented as Paper 85-1661 at the AIAA 18th Fluid Dynamics, Plasmadynamics and Lasers Conference, Cincinnati, OH, July 16-18, 1985; revision received Dec. 4, 1985.

created by imposing an electric field on the dielectric fluid is inversely proportional to the fifth power of the radius.[7] On Earth, the gravitational force is inversely proportional to the square of the radius. The effect of varying this power is needed to determine how capable the dielectric force is in simulating terrestrial gravity.

Physical Model

A schematic of the experimental setup is shown in Fig. 2. A dielectric fluid will be confined in a portion of the gap between the spheres by placing solid walls in the spherical domain. The annulus is subdivided to provide room for instrumentation. Temperature profiles imposed on the spheres by heaters will simulate the equator-to-pole distribution and establish the large-scale vertical stability (warmer outer sphere) of the atmosphere. The gravitational body force on the atmosphere is simulated by application of an electric field across the gap which generates a radial body force in the dielectric fluid. In order to be radial, this force requires the zero gravity environment of space, since the Earth's gravitational force would greatly distort the simulated gravitational force field.

The Numerical Model

The numerical model solves the axisymmetric incompressible Navier-Stokes equations in a vorticity/stream function formulation for a Boussinesq fluid. Boundary conditions appropriate for the AGCE were incorporated, i.e., the no-slip conditions and conducting walls. Details of the numerical model may be found in previous work.[8] A brief summary of the scheme is now given.

As stated earlier, the numerical model utilizes a mixed pseudospectral/finite difference scheme. Due to the presence of the latitudinal side walls (see Fig. 2), Tschebyschev polynomials are used as the spectral expansion functions. In addition, Tschebyshev collocation methods insure an exponential rate of convergence as opposed to the algebraic rates associated with finite-difference (FD) methods.[9] It was sufficient to use the pseudospectral formulation in only one direction (latitude) since the computational grid required 1/7 to 1/3 the number of grid points as the pure FD model.

The numerical scheme treats the rotation and advection terms explicitly while radial diffusion terms are implicitly solved. Pseudospectral derivatives are computed by setting up appropriate matrices for Tschebyshev collocation outside the time iteration process. Latitudinal derivatives are thus computed via a simple matrix multiplication at each time step.

The Poisson equation for stream function was solved in two ways. Initially a pseudotime derivative was introduced so that at steady state the Poisson equation would be satisfied. During this internal iteration latitudinal derivatives were not updated, which introduced a stabilizing factor in the scheme. This effective "pseudotime lag" in the Poisson iteration allowed the model to utilize a time step comparable to an implicit formulation in the overall iteration scheme. Alternatively, the matrix corresponding to the Laplacian operator was inverted by a conventional LU decomposition and back solution. Though a fewer number of steps were required in the latter formulation, a much more stringent time interval restriction was found necessary.

Numerical Model Application: Varying Experimental Parameters

The main results of an extensive parameter study which varied boundary temperatures and rotation rates for several gravitational force distributions will now follow. The latitudinal side walls were set at $\pi/4$ and $3\pi/4$. The inner and outer sphere radii were set at 5 and 6 cm, respectively. The term governing the force distribution is the buoyancy

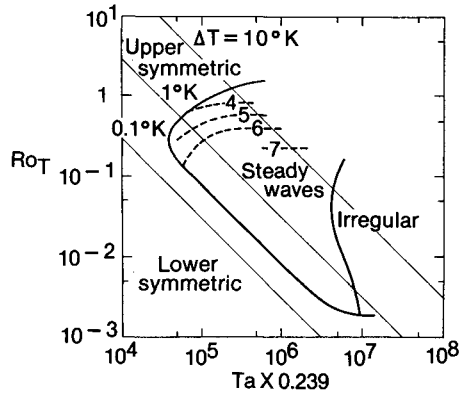

Fig. 1 Cylindrical annulus regime diagram.

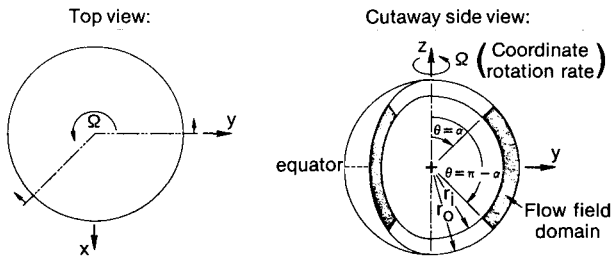

Fig. 2 Cutaway view of physical model.

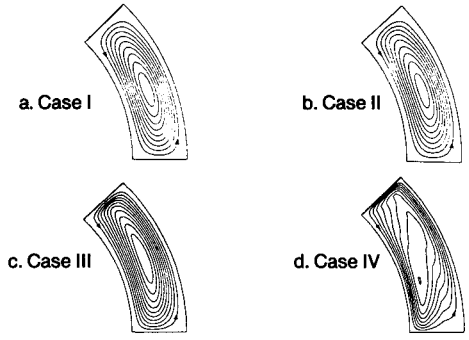

Fig. 3 Ψ contour plots for cases I to IV.

term of the vorticity equation[8] as given below:

$$\mathrm{GrEk}^2 \sin\theta \left(\frac{1}{r}\right)^n \frac{\partial T}{\partial \theta} \tag{3}$$

The gravitational distribution is varied by changing the exponent for $1/r$, and imposing that a mean value of gravity (g_{mean}) be maintained across the gap. Therefore Gr is defined in terms of a reference gravitational constant (g_{ref}):

$$\mathrm{Gr} = \frac{g_{\text{ref}} \alpha \Delta T r_0^3}{\nu^2} \tag{4}$$

where α and ν are the coefficients of thermal expansion and kinematic viscosity and ΔT is the maximum temperature difference on the boundaries. The constant g_{ref} is calculated as follows:

$$g_{\text{ref}} = 980(r_0 - r_i)\left[\int_{r_i}^{r_0} \left(\frac{r_0}{r}\right)^n \mathrm{d}r\right]^{-1} \tag{5}$$

where r_0 and r_i are the outer and inner sphere radius.

Table 1 Heat transfer ratios for increasing Grashof and Ekman numbers

Case	Gr	Ek	$GrEk^2$	$\frac{q_{\pi/4}}{q_{(\pi/4)c}}$[a]	$\frac{q_{\pi/2}}{q_{(\pi/2)c}}$	$\frac{q_{5\text{ cm}}}{q_{5c}}$	$\frac{q_{6\text{ cm}}}{q_{6c}}$
I	2.84×10^{3}	2.78×10^{-1}	219.2	1.0	0.0	1.0	1.0
II	2.84×10^{4}	2.78×10^{-2}	21.92	2.0	0.0	0.861	0.913
III	2.84×10^{5}	2.78×10^{-3}	2.192	8.8	0.0	0.566	0.890
IV	2.84×10^{6}	2.78×10^{-4}	0.2192	15.8	0.0	0.287	0.898

[a] q_c = heat transfer from conduction solution.

Cases I through IV, defined in Table 1, allow the study of the effect on the flowfield if Gr and Ek are allowed to vary by 4 orders of magnitude while maintaining a uniform gravitational field ($n=0$). Each of these quantities have physical significance. The Grashof number represents the ratio of buoyancy to viscous forces. If $Gr\neq0$, it couples each of the other equations through the vorticity equation. If $Gr=0$, the energy equation become uncoupled. The Ekman number measures the ratio of viscous to Coriolis forces in the flowfield, and multiplies the diffusive and buoyance terms.

Figures 3-6 are contour plots of stream function (Ψ), latitudinal velocity (u), vorticity (ξ), and temperature (T) for all four cases. Most noted in the contour plots is the increasing departure from symmetry. In addition, increased meridional transport for increasing Gr is evident in the Ekman layers of stream function (Fig. 3). The zonal jets seen in the contours of u (Fig. 4), are seen to move northward as buoyancy forces increase (higher Gr). Vorticity maxima are seen in Fig. 5 to shift from the inner radial wall at mid-latitudes for case I to the wall at $\pi/4$ and approximately 5.6 cm for case IV. Strong thermal boundary layers develop, as is evident in temperature contour plots of case IV, relative to the previous cases, which for case I is essentially a conduction profile (Fig. 6). These effects are all associated with an increasing buoyancy force that appears to be the dominant factor relative to increasing rotation by the same order of magnitude.

An interesting study regarding heat transfer rates for the four cases was made by carrying out a heat balance on the domain from $\pi/4$ to $\pi/2$ and from r_i to r_0. Ratios of the amount of heat transfer occurring at a given boundary over that occurring in pure conduction are listed in Table 1. The temperature isotherms of Figure 6c (case III) and 6d (case IV) indicate negative radial thermal gradients around $\theta=5\pi/12$ near the lower spherical wall. This is due to the increasing meridional motion for these two cases relative to cases I and II, which carry warm fluid northward as cold fluid sinks toward the equator. This motion acts to decrease the radial thermal gradients near the spherical walls and, for cases of strong meridional motion, even to reverse these gradients. The result is a decrease in the amount of heat transfer occurring at the spherical walls as evidenced in Table 1.

Results of varying n from 0, 2, and 5 to simulate a uniform, inverse square and inverse quintic gravitational field are shown in Fig. 7, which is a plot of stream function vs rotation rate (Ω). Three families of curves are shown corresponding to maximum temperature differences on the solid boundaries of 1, 2, and 3°C. Within each family ψ_{max} increases with n. For the parameter range studied, the effects of the gravitational distribution appear secondary relative to temperature and rotation.

However, Fig. 8 exhibits some characteristics of the flow which are influenced by the gravitational distribution. Figures 8a and 8b are stream function contours for a uniform field ($n=0$) and a field produced by the dielectric ($n=5$), respectively. Although overall features of the flowfields appear to be identical, the dielectric force produces a shift in the internal meridional recirculation relative to a uniform gravitational field. Note that the inner cell is stronger in the case of the dielectric than the inner recirculating cell of the uniform field. Conversely, the outer recirculating cell is stronger for $n=0$. Since the inverse quintic power law of the dielectric produces stronger forces toward the inner sphere which drop off quickly toward the outer sphere, this trend is expected.

To correlate the data, the Grashof number [Eq. (4)] was plotted against Ψ_{max} in Fig. 9 for the same cases given in Fig.

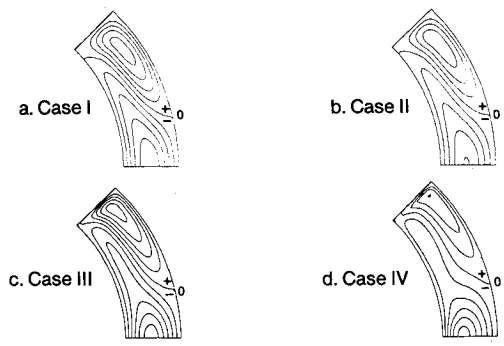

Fig. 4 u contour plots for cases I to IV.

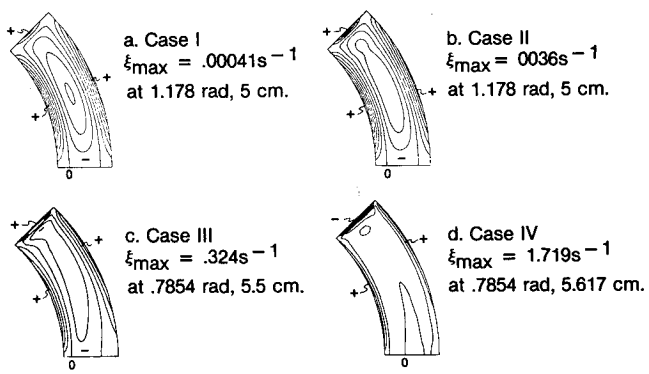

Fig. 5 ξ contour plots for cases I to IV.

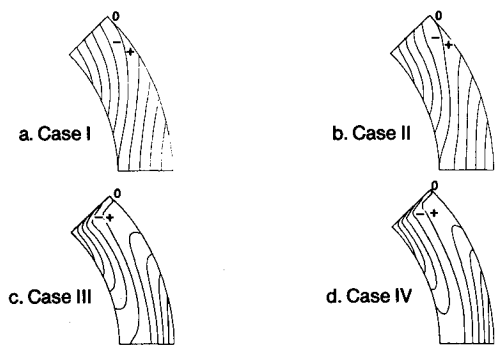

Fig. 6 T contour plots for cases I to IV.

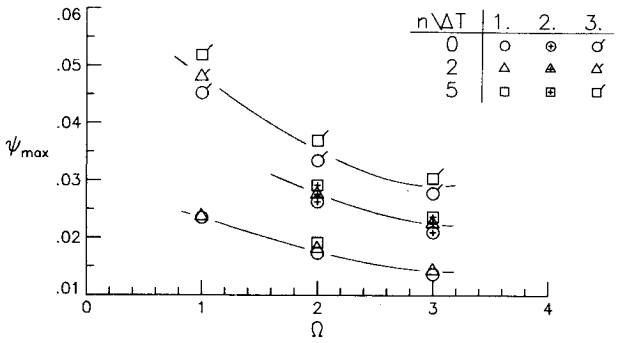

Fig. 7 Ψ_{max} vs Ω.

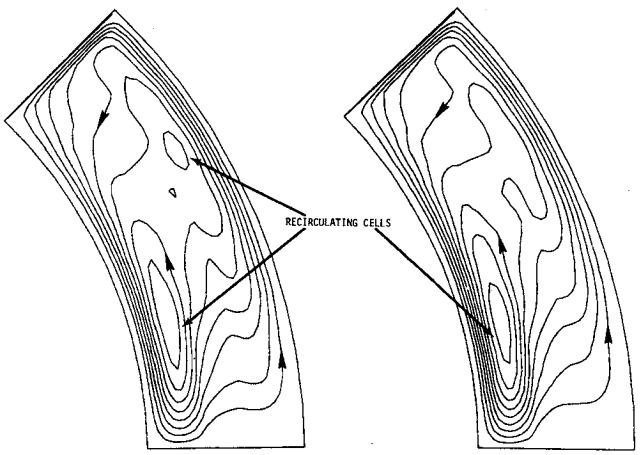

Fig. 8 Stream function contours (contour increment = 3×10^{-3}); a) $n=0$; b) $n=5$.

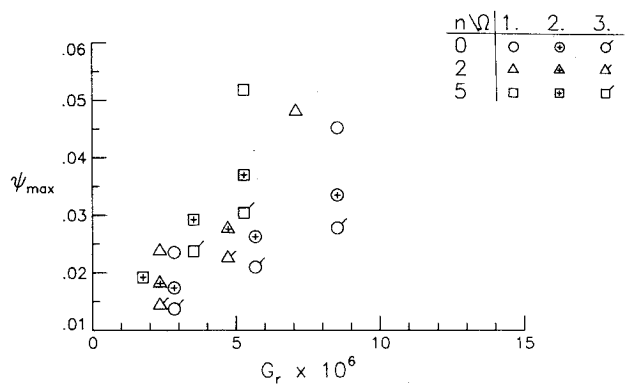

Fig. 9 Ψ_{max} vs Gr.

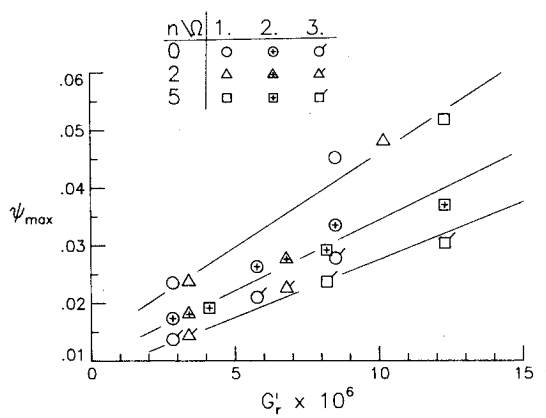

Fig. 10 Ψ_{max} vs Gr'.

7. The data are badly scattered. This Grashof number is the parameter obtained from nondimensionalizing the Navier-Stokes equations and imposes the proper condition in the buoyancy term, i.e., that the mean value of gravity across the gap be constant for varying n. However, it is clearly not the proper similarity parameter for this flow.

A modified Grashof number (Gr') is defined that takes into account the gravitational distribution as given by

$$\mathrm{Gr}' = \frac{\alpha \Delta T r_0^3 g_{\mathrm{mean}}}{(r_0 - r_i)\nu^2} \int_{r_i}^{r_0} \left(\frac{r_0}{r}\right)^n \mathrm{d}r \tag{6}$$

Figure 10 is a plot of ψ_{mean} vs Gr'. The scatter reduces considerably. The data collapse into three sets corresponding to a rotation rate of 1, 2, and 3 rad/s, respectively. For a given rotation rate, the data distribute themselves so that the highest temperature differences on the boundary correspond to the highest values of $\psi_{\max}$. For a given ΔT, the data show that as n increases from 0 to 5 $\Psi_{\max}$ also increases.

Discussion

It should be noted that at steady state no net torque is exerted on the fluid. Thus the sum of the viscous stresses exerted by the boundaries on the fluid should vanish. This means that the distribution of easterly and westerly flows at the boundaries should be about equal throughout the fluid volume. Such a trend is seen in the contour plots of azimuthal velocity (Fig. 4). However, the distribution of easterlies and westerlies in the atmosphere is different, which is expected since there is no outer boundary as is the case for the AGCE. Time-averaged atmospheric data yield the polar easterlies, the mid-latitude westerlies, and the tropical easterly trade winds. In the AGCE model, contour plots of azimuthal velocity reveal a region of positive zonal flow (westerlies) in the upper half of the domain, while the lower portion down to the equator shows negative zonal velocity (easterlies). Zonal linear speeds with respect to the Earth's surface can be computed by applying the principle of conservation of angular momentum for a unit mass. However, the observed wind speeds in the atmosphere are substantially less than those calculated on the basis of angular momentum conservation. It is believed that in the Earth's atmosphere the meridional flow breaks down into smaller circulations or cells.[10] Throughout the atmosphere the meridional components are on the average less than one-tenth of the zonal components. It was found in this numerical study that meridional flow values were on the average one-third of the zonal flow. The break-up of the meridional flow into two cells was noted to occur under specific conditions. At approximately the same location where temperature contours indicated a gradient reversal, the stream function contours were found to have two smaller cells in addition to the large cell representing the main meridional circulation. The reversal of the latitudinal gradient of temperature is certain to be a factor in causing these recirculations. It was noted that these recirculations were stronger for values of n equal to 0 and 2. Higher values of n were also found to increase flowfield values. It is possible that these higher values are due to the weakening of these recirculating cells in the meridional flow for the cases of $n=5$. Stream function contours show the appearance of these recirculations which are seen to be more prevalent for $n=0$ as opposed to $n=2$ and even less pronounced when $n=5$. Stream function contours where rotation was increased from 1 rad/s to 3 rad/s show the appearance of these smaller cells for increased rotation, which also inhibits meridional flow.

Conclusions

Experiments utilizing the dielectric force ($n=5$) should be observed with the knowledge that differences do exist between the resulting flowfield and a flow calculated with a

force proportional to $1/r^2$ (the Earth's gravitational force). Flowfield values will tend to be higher for the dielectric force. The meridional flow's breakup into two smaller cells, which has been observed in the atmosphere and shown numerically for the cases of $n=0$ and $n=2$, will be less pronounced for flows generated with a dielectric force. To compensate for these differences, rotation rates should be at least greater than 1 rad/s since meridional flow is inhibited by rotation. In addition, boundary temperature differences should not be too extreme so that internal temperature gradients will be weak enough to allow gradient reversals and subsequent recirculations in the meridional flow to occur.

It was found that the proper similarity parameter for correlating flows with different gravitational distributions is a modified Grashof number. This parameter was found to correlate a number of numerical experiments where rotation, boundary temperatures, as well as the gravitational distribution across the spherical gap, were all varied.

Varying the gravitational distribution was found to have minimal qualitative effects on a given flowfield. However, the dielectric force produces a shift in the internal meridional recirculations relative to a uniform gravitational field. The inner recirculating cell is stronger for the dielectric than for the uniform field, and conversely, the outer recirculating cell is stronger for the uniform field.

References

[1]Hide, R., "Some Experiments on Thermal Convection in a Rotating Liquid," *Quarterly Journal of the Royal Meteorological Society*, Vol. 79, Jan. 1953, p. 161.

[2]Fowlis, W. W. and Hide, R., "Thermal Convection in a Rotating Annulus of Liquid," *Journal of Atmospheric Science*, Vol. 22, Sept. 1965, pp. 541-558.

[3]Lorenz, E. N., "A Proposed Explanation for the Existence of Two Regimes of Flow in a Rotating Symmetrically-Heated Cylindrical Vessel," *Proceedings of the First Symposium on the Use of the Models in Geophysical Fluids*, Sept. 1953, pp. 73-80.

[4]Williams, G. P., "Thermal Convection in a Rotating Fluid Annulus: Part 1. The Basic Axisymmetric Flow," *Journal of Atmospheric Science*, Vol. 24, March 1967a, pp. 144-161.

[5]Williams, G. P., "Thermal Convection in a Rotating Fluid Annulus: Part 2," *Journal of Atmospheric Science*, Vol. 24, March 1967b, pp. 162-174.

[6]Miller, T. L. and Gall, R. L., "A Linear Analysis of the Transition Curve for the Baroclinic Annulus," *Journal of Atmospheric Science*, Vol. 40, Sept. 1983, pp. 2293-2303.

[7]Hart, J. E., "Studies of Earth Simulation Experiments," NASA CR-2753, 1976.

[8]Macaraeg, M. G., "A Mixed Pseudospectral/Finite Difference Method for the Axisymmetric Flow in a Heated, Rotating Spherical Shell," *Journal of Computational Physics*, Vol. 62, No. 2, Feb. 1986, pp. 297-320.

[9]Hussaini, M. Y., Streett, C. L., and Zang, T. A., "Spectral Methods for Partial Differential Equations," *Transactions of the First Army Conference on Applied Mathematics and Computing*, Aug. 1984, pp. 883-925.

[10]Byers, H. R., *General Meterology*, McGraw-Hill Book Co., Inc., New York, 1959.